

Melamine Barbiturate as a Light-Induced Nanostructured Supramolecular Material for a Bioinspired Oxygen and Organic Radical Trap and Stabilization

Alexandra A. Timralieva, Ivan V. Moskalenko, Pavel V. Nesterov, Vladimir V. Shilovskikh, Alexander S. Novikov, Elizaveta A. Konstantinova, Alexander I. Kokorin, and Ekaterina V. Skorb*



Cite This: *ACS Omega* 2023, 8, 8276–8284



Read Online

ACCESS |



Metrics & More

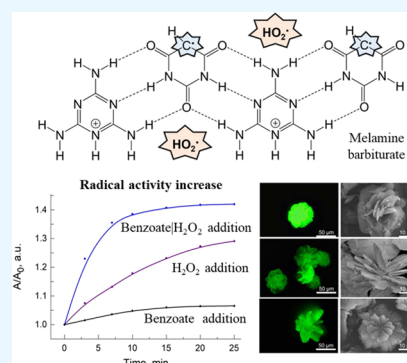


Article Recommendations



Supporting Information

ABSTRACT: Use of coantioxidant systems is a prospective way to increase the effectiveness of antioxidant species in tissue repair and regeneration. In this paper, we introduce a novel scheme of a reactive oxygen species (ROS) trap and neutralization during self-assembly of supramolecular melamine barbiturate material. The performed reaction chain mimics the biological process of ROS generation in key stages and enables one to obtain stable hydroperoxyl and organic radicals in a melamine barbiturate structure. Melamine barbiturate also neutralizes hydroxyl radicals, and the effectiveness of the radical trap is controlled with ROS scavenger incorporation. The number of radicals dramatically increases during light-inducing and depends on pH. The proposed scheme of the ROS trap and neutralization opens a way to the use of supramolecular assemblies as a component of coantioxidant systems and a source of organic radicals.



INTRODUCTION

Bioinspired material design has been a great trend in tissue engineering for at least a decade.^{1–4} One crucial aspect of tissue engineering is oxygen delivery or production that requires novel derivatives of previously known functional materials.⁵ Several metal–organic frameworks are considered to trap oxygen due to their high porosity and specific surface area.^{6–8} Some layered perovskites show the same function but without oxygen release.^{9,10} Bioinspired materials that mimic biological systems' functions or composition release oxygen under mild conditions, which is a great advantage of these materials.¹¹

A wide range of nanostructured biomaterials for tissue repair tends to respond only under external stimuli.¹² Some of them respond in the presence of O-centered radicals and turn into the activated state.^{13,14} On the other hand, O₂ delivery is often associated with undesired O-centered radicals' increase in the tissue, which requires antioxidant incorporation.¹⁵

O-centered radicals are a class of an oxygen-bearing species that commonly are extremely active. They play an important role in a wide range of biological processes, e.g., aging and age-dependent diseases.¹⁶ Both radical and nonradical oxygen derivatives can promote oxidizing. This class of substances is called reactive oxygen species (ROS), also called oxygen free radicals. This class includes both radical and nonradical substances. The first group includes superoxide (O₂^{•-}), hydroxyl (HO[•]), peroxy (ROO[•]), and hydroperoxyl (HO₂[•]) radicals. The second one consists of hydrogen peroxide (H₂O₂),

lipid hydroperoxide (ROOH), hypochlorous acid (HOCl), ozone (O₃), and singlet oxygen (¹O₂).¹⁷

The oxidizing function is not the same for O-centered radicals. The hydroperoxyl radical HO₂[•] greatly contributes to oxidation stress in living systems, while its conjugated base, superoxide O₂^{•-}, is inactivate as an oxidizing initiator.¹⁸ HO₂[•] initiates the lipid peroxidation of polyunsaturated fatty acids with the formation of unstable and reactive fatty acid molecules, which contribute to membrane and tissue damage.¹⁹ HO₂[•] contribution increases the rate constant of polyunsaturated fatty acid oxidation.²⁰

However, HO₂[•] is an important part of coantioxidant systems as it regenerates antioxidant agents such as nitroxides, phenols, amines, and quinones due to the fast hydrogen atom transfer (HAT).^{21–23} This approach, combined with antioxidant nanoparticle synthesis, enables the increase of antioxidant activity by several times.²⁴ A wide range of nanoparticles that produces antioxidant enzymes has been synthesized, but the question of HO₂[•] radical stability has still remained open.²⁵ One prospective way of stabilizing radicals is a noncovalent approach, e.g., the applicability of supramolecular materials as organic

Received: October 10, 2022

Accepted: January 27, 2023

Published: February 22, 2023



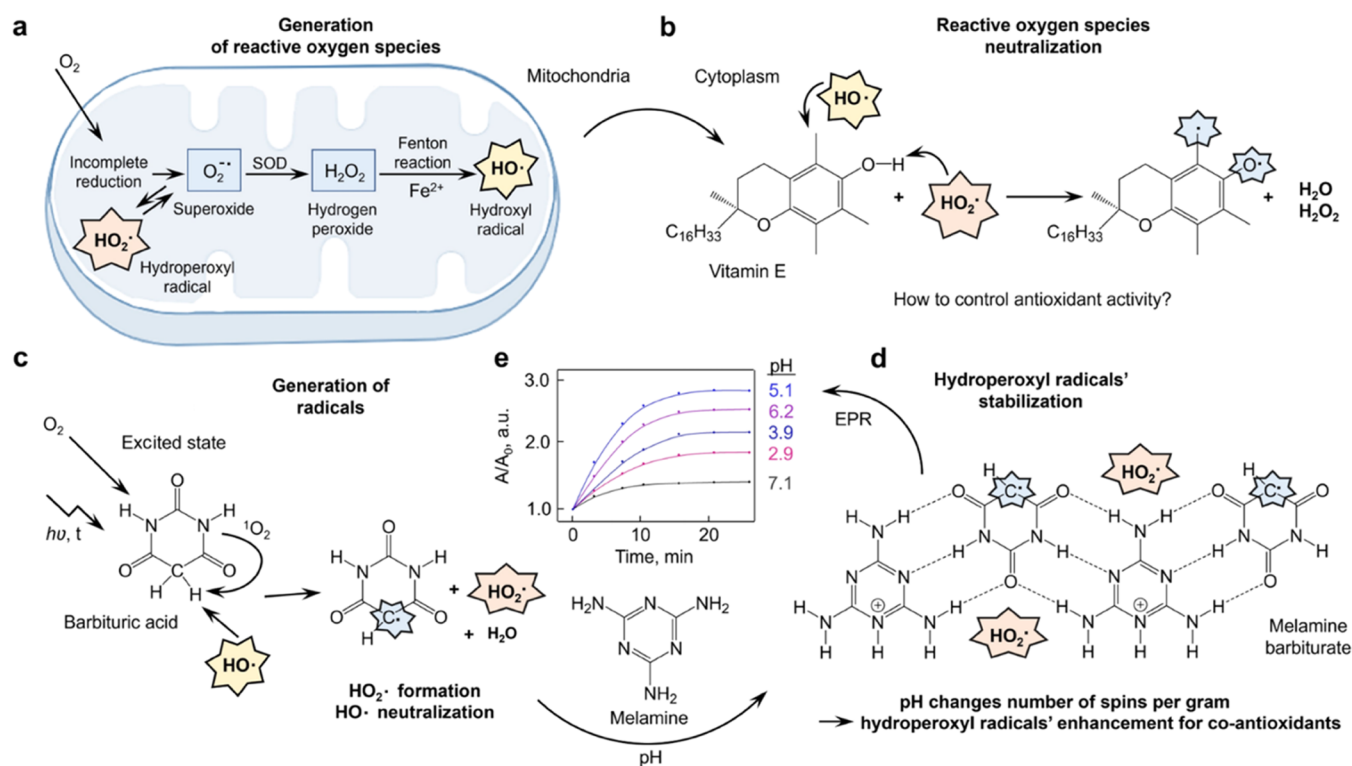


Figure 1. Reactive oxygen species production in mitochondria (a), and its neutralization by vitamin E in the cytoplasm (b). Bioinspired way of HO_2^\bullet generation and HO^\bullet neutralization by barbituric acid (c), and HO_2^\bullet trap and stabilization into the melamine barbiturate structure (d). Radical trap and formation depend on pH and light irradiation: EPR kinetic curves of the melamine barbiturate system under light irradiation at 298 K as a function of pH values (e).

radical cages.^{26,27} In previous studies, we had presented melamine barbiturate (M-B) supramolecular assembly as a nanostructured material that traps O-centered radicals and shows significant radical activity.^{28,29}

Here, we present an M-B behavior study in the presence of ROS and ROS scavengers to specify the radical's trap and stabilization function. Surprisingly, the process of melamine barbiturate assembly almost mimics ROS formation in the mitochondria and its further neutralization in the cytoplasm.

We propose melamine barbiturate as a novel material for hydroperoxyl radical trap for the purposes of stable radical storage and antioxidant regeneration. Besides, we show that melamine barbiturate can prevent the oxidation action of hydrogen peroxide and hydroxyl radical through organic radical formation in the M-B structure. Furthermore, light-induced radicals expand and the pH control of radical number is performed.

RESULTS AND DISCUSSION

According to the performed density functional theory (DFT) calculations,^{28,29} one radical center likely links up the O-centered radicals. The previously proposed $\text{O}_2^{\bullet-}$ is in equilibrium with its protonated form HO_2^\bullet in the aqueous medium. However, M-B crystalline aggregates go through thermal processing, and then their radical activity is measured. Heterogeneous uptake and stabilization are typical for HO_2^\bullet radicals in a nonaqueous medium.³⁰ Here, we present a batch of reactions for hydroperoxyl generation in M-B without corrections on $\text{O}_2^{\bullet-}$ formation.

The HO_2^\bullet radical can regenerate antioxidants such as phenols. Tocopherol as a methylated phenol is one of the active

compounds of the vitamin E group that occurs in plasma to prevent membrane damage by ROS.³¹ Hydroperoxyl and hydroxyl radicals form in the mitochondria during incomplete oxygen reduction and further reaction chain with superoxide dismutase (SOD) and Fe^{2+} ions (Figure 1a).³² HO_2^\bullet and HO^\bullet radicals relocate in the plasma via the mitochondrial electron transport chain and attack $-\text{OH}$ and $-\text{CH}_3$ functional groups of the tocopherol correspondingly (Figure 1b). As a result, both ROS are neutralized, and two organic radicals appear. In a real biological system, tocopherol stays as a radical and no more acts as an antioxidant, so its antioxidant activity is limited at all. The question of antioxidant activity control and increase stays open in the case of lipid membrane repair.

However, tocopherol radicals can be regenerated via fast hydrogen atom transfer (HAT) from initial HO_2^\bullet radicals.³³ For this purpose, a source of stable hydroperoxyl radicals is needed. We applied the performed scheme of ROS generation and neutralization to the M-B assembly process, and several similar key stages were indicated.

Barbituric acid (BA) as a single component shows no electron paramagnetic resonance signal, and a weak signal is observed during UV-light irradiation. Thus, we considered that light-inducing can be an essential stimulus for radical generation as was stated for a wide range of nanomaterials.^{34,35} UV-light irradiation promotes oxygen transition from the triplet state to the singlet state, while compounds with the carbonyl group in the excited state present in the reaction medium.^{36,37} BA has three carbonyl groups and easily goes into the excited state, so singlet oxygen formation is highly probable.³⁸ The reaction of BA with the formed singlet oxygen can theoretically go via two BA sites (Figure S1, top). It is thermodynamically preferable that singlet oxygen as a strong oxidizer takes the proton off the

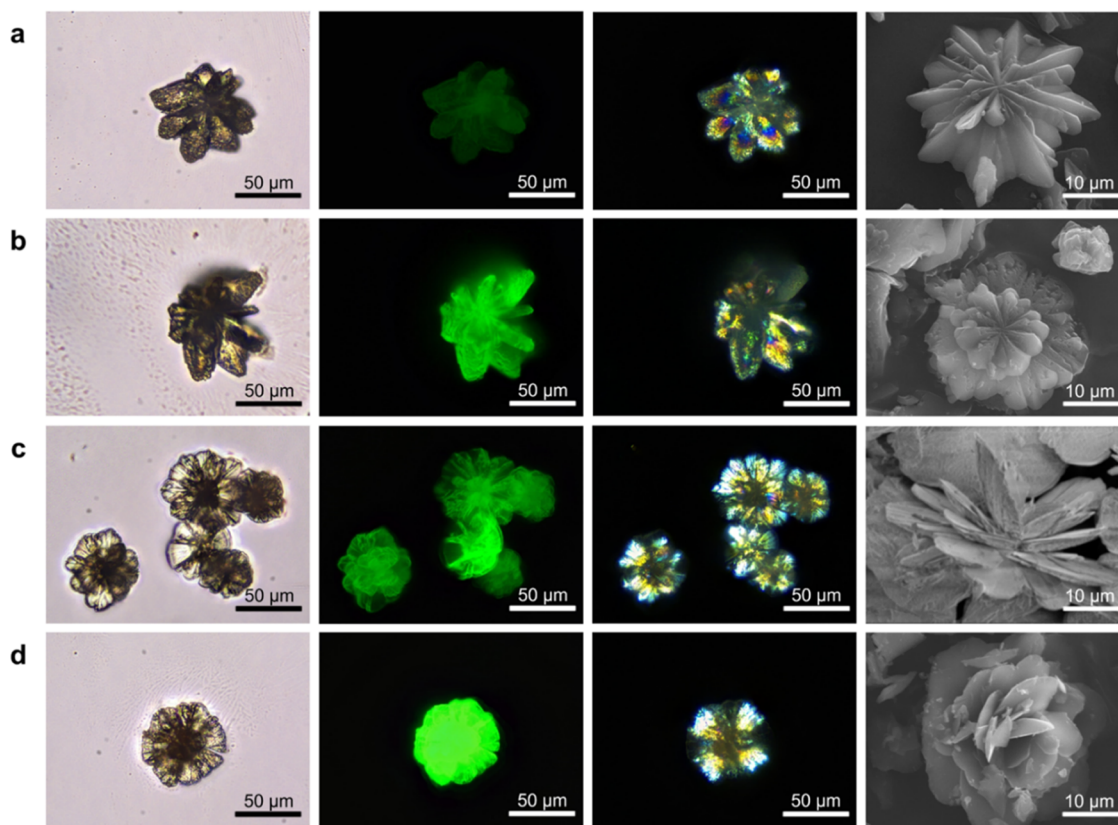
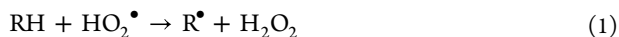


Figure 2. Melamine barbiturate (a), M-B formed in the presence of sodium benzoate (b), H_2O_2 (c), H_2O_2 and sodium benzoate (d): bright-field, FITC channel fluorescence, polarized light optical microscopy, and scanning electron microscopy (from left to right).

$-\text{CH}_2$. Energy is required, and a heating of up to $120\text{ }^\circ\text{C}$ can cover it during the experiment. It is in good accordance with X-ray diffraction data of M-B, which show deprotonated BA molecules in the structure.³⁹ The same calculations were conducted for melamine (M) oxidation and reactions with triplet oxygen (Figure S1, bottom). These reactions also are not energetically favorable.

Thus, BA produces an active HO_2^\bullet radical via the reaction chain with oxygen under light irradiation (Figure 1c), and this stage matches mitochondrial hydroperoxyl radical generation. An important difference is that BA produces no HO^\bullet radicals, and we decided to artificially add it to the M-B assembly.

When BA reacts with melamine (M), the hydroperoxyl radical is not stabilized yet and can act as an oxidizer via HAT



We calculated HAT of M and BA with both hydroperoxyl and hydroxyl radicals, in comparison. The HAT of M and BA via HO_2^\bullet is thermodynamically unfavorable at 298 K, while three reactions with HO^\bullet have significant negative ΔG values (Figure S2). Thus, the hydroperoxyl radical stays nonactive in M-B (Figure S2).

Figure 1d shows that there are stable hydroperoxyl radicals and organic radicals $-\text{CH}^\bullet$ at BA molecules in the M-B assembly. We consider that not only the $-\text{CH}^\bullet$ radical can occur in M-B but also $-\text{C}^\bullet$ if BA is deprotonated during the assembly. This stage is similar to ROS neutralization in the plasma. Despite the rigidity of HO_2^\bullet in M-B, it can become active in the presence of other agents. Thus, we propose using M-B as the regenerating agent for antioxidant systems.

However, the question of the controllable increase of the HO_2^\bullet radical number still remains significant. As was confirmed in previous research, the M-B radical activity depends on pH values. At first, we decided to determine the optimal conditions for M-B formation. EPR measurements were conducted for M-B samples prepared at five different pH values. As an example, Figure S3 presents the experimental EPR spectra of M-B recorded at 298 K before and after 20 min of light irradiation prepared at pH 3.9 and 6.2 and also a sample of M-B + 2.0% H_2O_2 . One can see that there are at least two radical centers in the M-B complex, whose nature has been presumably discussed in refs 28, 29. Symbols R_I , R_{II} , and R_2 in Figure S3 show line positions of two stable free radicals, most likely HO_2^\bullet (R_I , R_{II}) and C^\bullet (R_2), probably CH^\bullet centers, in BA correspondingly. The samples were irradiated by UV light during 25 min, and the ratio of the total radical signal intensity after and before irradiation was calculated for each sample. The radical signal intensity increases by about 2 times in cases of pH = 6.2 and 5.1 (Figure 1e). This effect is related most likely to the protonation and deprotonation of functional groups of melamine (M) and barbituric acid (BA) and the locked site for singlet oxygen attack. For further research, pH = 6.2 was considered the most preferable condition as it almost matches the pH value of the M-B suspension after complete formation, and no extra treatment is required.

It should be noted that EPR line intensities sufficiently change under illumination (Figure S3). Indeed, it is evidently seen that the intensity of the R_2 line noticeably increases in the case of spectra (b) and (d) in comparison with spectra (a) and (c) in parallel to the amplitude of the whole spectrum. Therefore, we

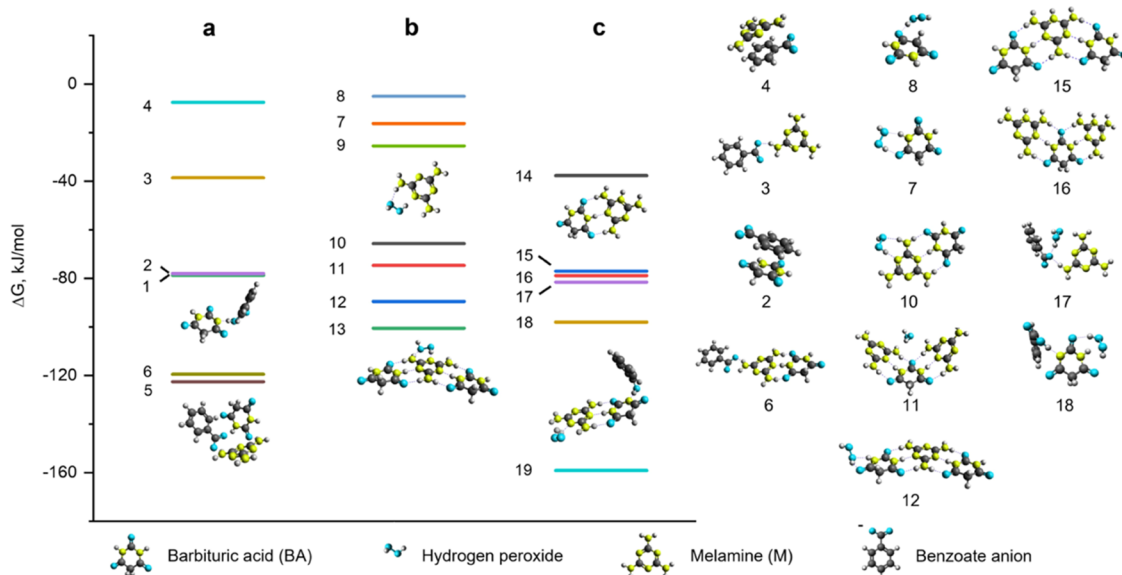


Figure 3. Change of Gibbs free energy during associate formation of M, B with the benzoate anion (a), H_2O_2 (b), and both benzoate anion and H_2O_2 in contrast to melamine barbiturate dimers and trimers (c).

may conclude that UV–vis light irradiation results in the generation of new C^\bullet radicals in the M-BA system.

DFT calculations showed that HO^\bullet preferably reacts with the $-\text{CH}_2$ site of BA via HAT. Theoretically, it means that M-B can convert HO^\bullet into H_2O during M-B treatment with the hydroxyl radical source. As has been mentioned before, EPR spectra show that there are two radical centers in M-B. The first type of such a center is definitely the HO_2^\bullet radical. The second one likely links up C-centered radicals, most probably, CH^\bullet of BA. Thus, HO^\bullet treatment of M-B should increase the total radical activity due to the CH^\bullet expansion, which is in agreement with EPR data.

To confirm this statement, we obtained M-B samples prepared from solutions of M and BA containing 2 wt % H_2O_2 as a source of hydroxyl radicals. To check the effect of hydroxyl radicals, we conducted experiments with 0.05 wt % sodium benzoate as the HO^\bullet scavenger. The control experiment with sodium benzoate was also performed. The suspensions of M-B were centrifuged, the precipitates were dried at 120°C and rewashed with deionized water, and the procedure was repeated three times to remove traces of H_2O_2 and sodium benzoate.

The obtained crystalline aggregates show changes in the M-B morphology (Figure 2). Bright-field optical microscopy images demonstrate that the size distribution of M-B remains almost the same, but the shape changes. In the case of pure M-B and the adding of sodium benzoate, aggregates show an eight-star shape with strong twinning from the center. Sodium benzoate presence leads to a high increase of surface defects. Two samples of M-B that formed in the presence of H_2O_2 are also aggregates with strong twinning. The main difference is the rose-like shape consisting of thin platelets. Platelets become thinner, to $1\ \mu\text{m}$ thickness, from the bottom of the aggregate to its top. Each platelet is represented by a single crystal. M-B formed in the presence of sodium benzoate consists of a hexagonal prism with triangular pyramidal head single crystals also as pure M-B aggregates.

MB aggregates show distinct anisotropy in cross-polarized light. In general, separate single crystals exhibit uniform extinction when rotated in polarized light. The light extinction has a radially radiant form, which indicates the presence of a

clear crystallization center. This makes it possible to attribute the formation of such aggregates to systems with nucleation control and high nucleation energy relative to that of the stationary growth process.⁴⁰

All samples show luminescence at 517 nm under light irradiation (495 nm, FITC channel). Pure M-B has a weak luminescence with a raise at the edges of single crystals. Luminescence becomes stronger when M-B forms in the presence of sodium benzoate, and the maximum is observed at both the edges and surface defects of aggregates. We associate the luminescence of M-B with radical contribution to the π -system and electron localization.⁴¹ Surface binding of luminescence is considered to depend on the number of radicals taken up by surface defects.

In the case of H_2O_2 , luminescence is also pronounced mostly on the edges of platelets where the number of defects is the most. When we add sodium benzoate to H_2O_2 , the formed M-B shows a dramatic increase of luminescence among all of the aggregates. We also see that the luminescence strengthens at the edges of each platelet. The number of platelets is significantly more than for the M-B formed in the presence of only H_2O_2 . Often, we also observe the increase of defects on the M-B surface in the case of small aggregates like it occurs when we add only sodium benzoate.

Four samples were analyzed by X-ray powder diffraction (XRD) in comparison to initial compounds (Figure S4). No traces of M, BA, and sodium benzoate fractions are observed. For all M-B samples, we obtained similar reflex patterns, but the plane (002) extremely increases in the case of sodium benzoate addition. According to the previous study, sodium benzoate can be incorporated into the structure of M-B with the mentioned increase in interplanar spacing.

Figure S4A also shows that a little reflex appears in the case of H_2O_2 addition. We suppose that some structural changes can occur; however, the intensity of the reflex is too small to correctly interpret it. The calculated crystallinity values decrease to 87.1 and 63.0% for pure M-B and M-B formed in the presence of H_2O_2 , respectively. Amorphous phases are 29.1 and 32.4% for M-B formed with only sodium benzoate and both sodium

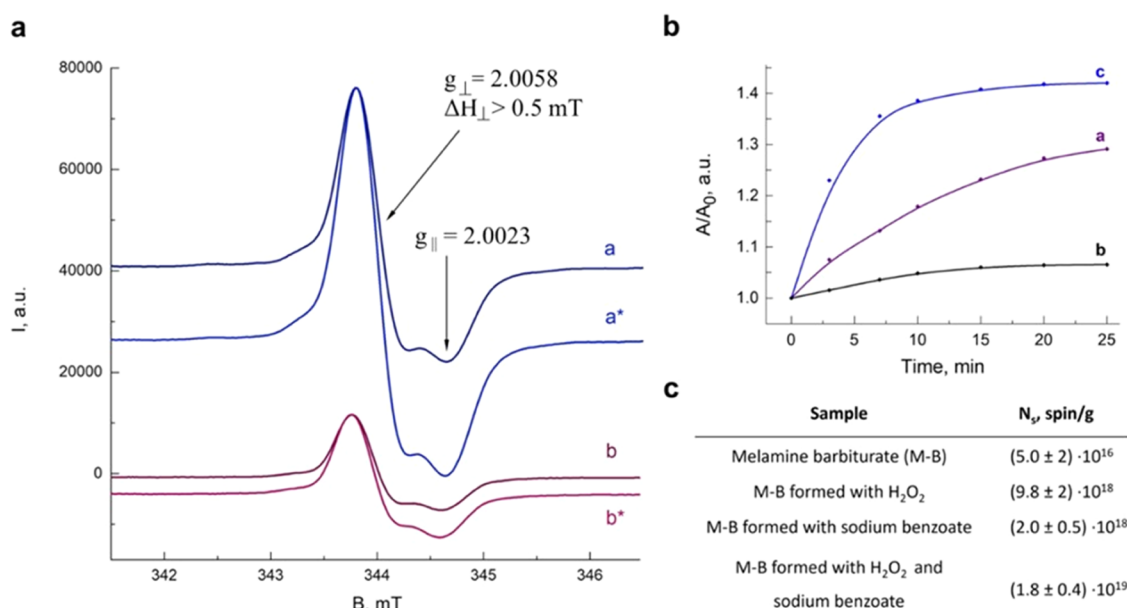


Figure 4. (Panel a) EPR spectra of M-B samples formed in the presence of H_2O_2 (a) and sodium benzoate (b) before and after 20 min of light irradiation (*) at $T = 298 \text{ K}$. (Panel b) Kinetic curves at 298 K under light irradiation of M-B samples obtained in the presence of H_2O_2 (a), sodium benzoate (b), and both H_2O_2 and sodium benzoate (c). (Panel c) Total concentration of spins in the dark at $T = 298 \text{ K}$ in M-B samples obtained at $\text{pH} = 6.2$.

benzoate and H_2O_2 , respectively. It seems that sodium benzoate promotes overgrowth of M-B and, as a result, a decrease in crystallinity.

To assess whether sodium benzoate incorporates into the M-B structure, we modeled several associates via DFT calculations, and values of Gibbs free energy change during associates' formation of M, B, H_2O_2 , and benzoate anion were obtained (Figure 3). Formation of melamine and benzoate anion associates (M-Benz) such as structures 3 and 4 is less thermodynamically favorable than BA-Benz (structures 1, 2). During BA-Benz formation, it was observed that the hydrogen atom transfers from the N-H bond of BA to the $-\text{COO}^-$ functional group. M-B-Benz trimers (structures 5, 6) also form with a decrease in the Gibbs free energy in contrast to melamine barbiturate dimers and trimers (structures 14, 15, 16). The benzoate anion association with BA via a hydrogen bond (structure 5) is more thermodynamically favorable for trimers.

The H_2O_2 hypothetically can associate with BA in two ways (structures 7, 8), and structure 8 is the least thermodynamically favorable. H_2O_2 association with M (structure 9) occurs preferably than with BA. H_2O_2 association with the M-B dimer (structure 10) is thermodynamically favorable, and H_2O_2 coordinates preferably to M than to BA. H_2O_2 association with M-B trimers (structures 11, 12, 13) is thermodynamically favorable. Note that despite numerous attempts to obtain an equilibrium structure 12, corresponding to the supramolecular associate of BA with the benzoate anion, as a result of geometry optimization, an associate 12', corresponding to the barbiturate anion and benzoic acid, was always obtained (see the attached animation of the geometry optimization steps for one of the attempts, in which BA and the benzoate anion in the starting geometry are spaced by 3 Å). H_2O_2 coordination to M in B-M-B (structure 13) leads to a significant gain in the Gibbs free energy of formation in contrast to all other calculated associates. According to DFT calculations, H_2O_2 and sodium benzoate possibly associate with M and BA during melamine barbiturate formation in experiments performed above. DFT calculation

results correspond to XRD data that sodium benzoate likely temporarily incorporates into the M-B structure. Molecular dynamics simulations show that M-Benz and BA-Benz associates exist and the M-BA dimer seems more stable and has a longer life period (Figure S5). Moreover, BA-Benz dimers have a longer life period than M-Benz dimers, but the interaction between barbituric acid and sodium benzoate can go only after melamine barbiturate formation as this interaction is less preferable. Breaking of barbituric acid and benzoate anion interaction through the washing of the process and explains the defects. Molecular dynamics simulation also shows that M-Na dimers exist but have a much smaller period of life. However, it seems that BA-Na does not exist in the solution or has a negligible period of life (Figure S6). The stability of M-B and H_2O_2 associates casts a doubt, but microscopy images confirm that the growth of M-B crystals is blocked for one axis.

We recorded four M-B samples using EPR to assess whether the radical's chemical redox activity also changes. One can see from Figure 4a that the type of the EPR spectrum shape is similar in all cases of studied samples, while their amplitudes and integral intensities differ much initially and also after light irradiation as shown by their kinetic curves (Figure 4b). Characteristic EPR parameters such as g -values g_{\perp} and g_{\parallel} as well as the line width ΔH_{\perp} were estimated and are shown in Figure 4a. Both sodium benzoate and H_2O_2 revealed a strong effect on the concentration of the created stable radicals. Measured total concentrations were performed (Figure 4c). M-B samples formed in the presence of H_2O_2 , sodium benzoate, and both reagents show an increase in the number of spins almost in 3 orders in contrast to the pure M-B sample. Considering the accuracy, we see that the M-B formed with both reagents shows almost the same increase of spin amount as the M-B formed with H_2O_2 .

We associate the difference with targeted activation of specific radical centers via sodium benzoate and hydrogen peroxide. H_2O_2 seems to increase the amount of stable CH^{\bullet} radicals according to the scheme shown above, while hydrogen peroxide

decomposes into HO• radicals. Sodium benzoate likely increases the amount of both stable CH• and HO₂• radicals. As was shown by microscopy methods, sodium benzoate increases the overgrowth of M-B and surface defects' appearance. It leads to an increase in the triplet oxygen number near the nucleation center and further trapped HO₂•. Expansion of two stable radicals explains the strong effect on the spin concentration, but it limits with the singlet oxygen formation stage.

However, sodium benzoate reduces the decomposition of H₂O₂ and weakens the effect of HAT between HO• radicals and BA molecules. It explains the smaller gain in the spin concentration than we expected for M-B samples formed in the presence of both sodium benzoate and H₂O₂. UV–Vis light illumination intensifies HAT that was blocked before and explains the difference in kinetic curves.

CONCLUSIONS

In this study, we performed a nanostructured supramolecular melamine barbiturate assembly for bioinspired radical trap, neutralization, and stabilization. The melamine barbiturate supramolecular assembly generates hydroperoxyl radicals via a light-induced reaction chain. The HO₂• radical remains stable in the M-B structure and seems to be activated as an antioxidant regenerator. An equilibrium between the hydroperoxyl radical and the superoxide radical can occur, and the presence of two conjugated radicals in M-B is probable. Moreover, the superoxide radical is also considered an effective oxidant regenerator as well as a hydroperoxyl radical.⁴²

Barbituric acid is oxidized with CH• radicals' formation that are stabilized into melamine barbiturate. Besides, oxidation of barbituric acid involves a singlet oxygen and neutralizes it as well. Thus, melamine barbiturate traps HO₂• radicals and generates CH• radicals.

We show that addition of reactive oxygen species such as H₂O₂ leads to a significant increase in radical activity. Melamine barbiturate neutralizes HO• radicals via hydrogen atom transfer with the increase in CH• radicals.

Addition of sodium benzoate intensively promotes HO₂• radical trapping even while H₂O₂ and HO• radicals are neutralized. Besides, the amount of spin increases by 1.4 times during UV–vis light irradiation.

Thus, in this study, we show a novel scheme of ROS stabilization and neutralization with supramolecular materials for antioxidant activity increase. The performed reaction chains mimic biological processes such as mitochondrial ROS generation and their neutralization in key stages.

EXPERIMENTAL SECTION

Materials. Melamine (M), barbituric acid (BA), and sodium benzoate were purchased from Sigma-Aldrich, and hydrogen peroxide (H₂O₂) was purchased from Lenreactiv. The chemicals were used without further purification: BA (C₄H₄N₂O₃, 99.0%, Sigma-Aldrich), M (C₃H₆N₆, 99.0%, Sigma-Aldrich), sodium benzoate (C₆H₅COONa, 99.0%, Sigma-Aldrich), and H₂O₂ (35%, Lenreactiv). Deionized water (18 MΩ·cm²/cm) was used as a solvent.

Synthesis. Stock 20 mm solutions of M and BA in water were prepared in advance to obtain four samples. Solutions were mixed and vigorously stirred in a 1:1 volumetric ratio to obtain a pure M-B suspension. The suspension was centrifuged, and the precipitate was dried at 120 °C and rewashed with deionized

water; this procedure was repeated three times to remove traces of initial compounds. Sodium benzoate powder was weighed to get 0.05 wt % in solution. Each stock solution was mixed with sodium benzoate powder and heated until powder dissolution. Solutions of M and BA with sodium benzoate were mixed, and the suspension was proceeded according to the above-mentioned protocol. First, 35% H₂O₂ was mixed with each stock solution to obtain solutions of M and BA in 2% H₂O₂. Solutions were mixed to obtain a suspension, and the following steps were the same as mentioned previously. Then, 35% H₂O₂ was diluted in 8.75 times; sodium benzoate was added to get a 0.1 wt % solution, and it was heated until powder dissolution. The obtained solution was mixed with each stock M and BA solution in a 1:1 volumetric ratio, and solutions of M and BA in H₂O₂ with sodium benzoate were mixed. Further steps were performed according to the procedure mentioned before.

Microscopy and Microanalysis. All of the prepared powders were investigated by means of optical and scanning electron microscopies. Microimages were acquired using a Zeiss Axio Imager.A2m. A Tescan Vega 3 scanning electron microscope equipped with an Oxford x-act energy-dispersive X-ray spectrometer was used for imaging and microanalysis. Operating conditions were as follows: 5 kV accelerating voltage, 100 s dwell time per spectrum. All data were processed using Oxford Aztec One software. Image analysis was performed using ImageJ software.

XRD. Powder diffraction data of M-BA, M-BA-Benz, M-BA-H₂O₂, M-BA-Benz-H₂O₂, and reference M, BA, and Benz were collected by means of D2 PHASER (Bruker) with Cu Kα radiation from the 5 to 60° angular range with a 0.02 step size and 1 s resonance time. Phase analysis was carried out using the software package Eva (Bruker) utilizing the ICSD crystal database (PDF4+).

EPR Measurements. The EPR spectra were recorded at room temperature with a Bruker spectrometer ELEXSYS-E500 (X-band, sensitivity up to 1010 spin/G). For investigating the photoactivity and behavior of paramagnetic centers (PCs), the samples were illuminated directly in the cavity of the spectrometer with the use of a 50 W high-pressure mercury lamp. The concentration of PCs was evaluated using a CuCl₂·2H₂O monocrystal with a known number of spins as the standard. The EPR spectra simulation permitting determination of *g*-factor values of radicals was carried out with the use of the EasySpin MATLAB toolbox. EPR spectra analysis was carried out using a computer program package developed by Prof. A. Kh. Vorob'ev (Chemistry Department, M. Lomonosov Moscow State University) and kindly provided to us.

Quantum Chemical Computations. The full geometry optimization of all model structures was carried out at the B3LYP-d3/def2-SVP level of theory utilizing the ORCA 5.0.3 program package.⁴³ Spin-restricted approximation for structures with closed electron shells and the unrestricted approach for structures with open electron shells have been employed. The RIJCOSX approximation utilizing the def2-SVP/C auxiliary basis set was employed.^{44,45} The convergence tolerances for geometry optimization were energy change = 5.0 × 10⁻⁶ Eh, maximal gradient = 3.0 × 10⁻⁴ Eh/Bohr, RMS gradient = 1.0 × 10⁻⁴ Eh/Bohr, maximal displacement = 4.0 × 10⁻³ Bohr, and RMS displacement = 2.0 × 10⁻³ Bohr. The couple perturbed self-consistent field (CPSCF) equations were solved using the conjugated gradient (CG) method with convergence tolerance on a residual of 1.0 × 10⁻⁶ Eh. The Hessian matrices were calculated for all optimized model structures to prove the

location of correct stationary points on the potential energy surfaces (no imaginary frequencies were found in all cases) and to estimate the thermodynamic properties (viz. enthalpy, entropy, and Gibbs free energy) for all model systems at 298.15 K and 1 atm.

Molecular Dynamics Simulations. MD simulations of M-BA association with Rh6G were performed utilizing the GROMACS program package⁴⁶ for topology preparation and OpenMM⁴⁷ for calculation. Interatomic interactions were described by the OPLS-AA/CM1A force field,⁴⁸ with topology and charges generated by LigParGen.^{49–51} For the water model, the rigid nonpolarizable TIP3P⁵² model was used. The cutoff for nonbonded and long-range interactions was 1.2 nm. For the calculation of long-range Coulomb interactions, the particle-mesh Ewald method was used.⁵³ Energy minimization was performed with the steepest descent algorithm. Simulations were performed in the NPT ensemble at $T = 300$ K and $P = 1$ atm in the cubic unit cell ($\sim 85 \times 85 \times 85 \text{ \AA}^3$). The integration time step for trajectories' calculations was 2 fs, and for relaxation, it was 0.5 fs. Radial distribution functions, spatial distribution functions, and dimer existence autocorrelation functions were calculated from the resulting trajectories using the TRAVIS program package.⁵⁴

■ ASSOCIATED CONTENT


SI Supporting Information

The Supporting Information is available free of charge at <https://pubs.acs.org/doi/10.1021/acsomega.2c06510>.

Additional animation for illustration of geometry optimization steps for barbituric acid and benzoate anion adduct, in which barbituric acid and benzoate anion in the starting geometry are spaced by 3 Å (MP4) Additional figures for illustration of pathways of M and BA oxidation via oxygen; corresponding calculated Gibbs free energies of reactions and equilibrium constants; HAT from BA and M to hydroperoxyl and hydroxyl radicals; corresponding calculated Gibbs free energies of reactions; and XRD data of four M-B samples (PDF)

■ AUTHOR INFORMATION

Corresponding Author

Ekaterina V. Skorb – *Infochemistry Scientific Center of ITMO University, St. Petersburg 191002, Russia*;  orcid.org/0000-0003-0888-1693; Email: skorb@itmo.ru

Authors

Alexandra A. Timralieva – *Infochemistry Scientific Center of ITMO University, St. Petersburg 191002, Russia*

Ivan V. Moskalenko – *Infochemistry Scientific Center of ITMO University, St. Petersburg 191002, Russia*

Pavel V. Nesterov – *Infochemistry Scientific Center of ITMO University, St. Petersburg 191002, Russia*

Vladimir V. Shilovskikh – *Infochemistry Scientific Center of ITMO University, St. Petersburg 191002, Russia*

Alexander S. Novikov – *Infochemistry Scientific Center of ITMO University, St. Petersburg 191002, Russia*

Elizaveta A. Konstantinova – *Physics Department, M. V. Lomonosov Moscow State University, Moscow 119991, Russia; Institute of Nano-, Bio-, Information, Cognitive and Socio-humanistic Sciences and Technologies, Moscow Institute of Physics and Technology, Dolgoprudny 141701 Moscow Region, Russia*

Alexander I. Kokorin – *Infochemistry Scientific Center of ITMO University, St. Petersburg 191002, Russia; N. N. Semenov Federal Research Center for Chemical Physics, Russian Academy of Sciences, Moscow 119991, Russia; Plekhanov Russian University of Economics, Moscow 115093, Russia*

Complete contact information is available at:

<https://pubs.acs.org/doi/10.1021/acsomega.2c06510>

Notes

The authors declare no competing financial interest.

■ ACKNOWLEDGMENTS

The work was carried out with the support of the Ministry of Science and Higher Education of the Russian Federation (agreement No 075-15-2021-1349) and was performed partially within the framework of the Program of Fundamental Research of the Russian Federation (Reg. No. 122040500068-0). Priority 2030 is acknowledged for infrastructural support.

■ REFERENCES

- (1) Zhang, D.; Chen, Q.; Bi, Y.; Zhang, H.; Chen, M.; Wan, J.; Shi, C.; Zhang, W.; Zhang, J.; Qiao, Z.; Li, J.; Chen, S.; Liu, R. Bio-Inspired Poly-DL-Serine Materials Resist the Foreign-Body Response. *Nat. Commun.* **2021**, *12*, No. 5327.
- (2) Molinaro, R.; Corbo, C.; Martinez, J. O.; Taraballi, F.; Evangelopoulos, M.; Minardi, S.; Yazdi, I. K.; Zhao, P.; de Rosa, E.; Sherman, M. B.; de Vita, A.; Toledano Furman, N. E.; Wang, X.; Parodi, A.; Tasciotti, E. Biomimetic Proteolipid Vesicles for Targeting Inflamed Tissues. *Nat. Mater.* **2016**, *15*, 1037–1046.
- (3) Wang, Y.; Xu, Y.; Zhai, W.; Zhang, Z.; Liu, Y.; Cheng, S.; Zhang, H. In-Situ Growth of Robust Superlubricated Nano-Skin on Electrospun Nanofibers for Post-Operative Adhesion Prevention. *Nat. Commun.* **2022**, *13*, No. 5056.
- (4) Fernandes, M. M.; Correia, D. M.; Ribeiro, C.; Castro, N.; Correia, V.; Lanceros-Mendez, S. Bioinspired Three-Dimensional Magnetoactive Scaffolds for Bone Tissue Engineering. *ACS Appl. Mater. Interfaces* **2019**, *11*, 45265–45275.
- (5) Li, Y.; Lou, N.; Xu, D.; Pan, C.; Lu, X.; Gan, L. Oxygen-Delivery Materials: Synthesis of an Open-Cage Fullerene Derivative Suitable for Encapsulation of H₂O₂ and O₂. *Angew. Chem.* **2018**, *130*, 14340–14344.
- (6) Lyu, J.; Zhang, X.; Chen, Z.; Anderson, R.; Wang, X.; Wasson, M. C.; Bai, P.; Guo, X.; Islamoglu, T.; Gómez-Gualdrón, D. A.; Farha, O. K. Modular Synthesis of Highly Porous Zr-MOFs Assembled from Simple Building Blocks for Oxygen Storage. *ACS Appl. Mater. Interfaces* **2019**, *11*, 42179–42185.
- (7) DeCoste, J. B.; Weston, M. H.; Fuller, P. E.; Tovar, T. M.; Peterson, G. W.; LeVan, M. D.; Farha, O. K. Metal-Organic Frameworks for Oxygen Storage. *Angew. Chem., Int. Ed.* **2014**, *53*, 14092–14095.
- (8) Moghadam, P. Z.; Islamoglu, T.; Goswami, S.; Exley, J.; Fantham, M.; Kaminski, C. F.; Snurr, R. Q.; Farha, O. K.; Fairen-Jimenez, D. Computer-Aided Discovery of a Metal-Organic Framework with Superior Oxygen Uptake. *Nat. Commun.* **2018**, *9*, No. 1378.
- (9) Kalapsazova, M. L.; Kostov, K. L.; Kukeva, R. R.; Zhecheva, E. N.; Stoyanova, R. K. Oxygen-Storage Materials to Stabilize the Oxygen Redox Activity of Three-Layered Sodium Transition Metal Oxides. *J. Phys. Chem. Lett.* **2021**, *12*, 7804–7811.
- (10) Klimkowicz, A.; Świerczek, K.; Rzaśa, T.; Takasaki, A.; Dabrowski, B. Oxygen Storage Properties and Catalytic Activity of Layer-Ordered Perovskites BaY1-XGdxMn2O5+δ. *Solid State Ionics* **2016**, *288*, 43–47.
- (11) Fu, X.; Ohta, S.; Kawakatsu, T.; Kamihira, M.; Sakai, Y.; Ito, T. Bioinspired Perfluorocarbon-Based Oxygen Carriers with Concave

- Shape and Deformable Shell. *Adv. Mater. Technol.* **2022**, *7*, No. 2100573.
- (12) Gelmi, A.; Schutt, C. E. Stimuli-Responsive Biomaterials: Scaffolds for Stem Cell Control. *Adv. Healthcare Mater.* **2021**, *10*, No. 2001125.
- (13) Lv, W.; Xu, J.; Wang, X.; Li, X.; Xu, Q.; Xin, H. Bioengineered Boronic Ester Modified Dextran Polymer Nanoparticles as Reactive Oxygen Species Responsive Nanocarrier for Ischemic Stroke Treatment. *ACS Nano* **2018**, *12*, 5417–5426.
- (14) Liu, Z.; Simchick, G. A.; Qiao, J.; Ashcraft, M. M.; Cui, S.; Nagy, T.; Zhao, Q.; Xiong, M. P. Reactive Oxygen Species-Triggered Dissociation of a Polyrotaxane-Based Nanochelator for Enhanced Clearance of Systemic and Hepatic Iron. *ACS Nano* **2021**, *15*, 419–433.
- (15) Willemsen, N. G. A.; Hassan, S.; Gurian, M.; Li, J.; Allijn, I. E.; Shin, S. R.; Leijten, J. Oxygen-Releasing Biomaterials: Current Challenges and Future Applications. *Trends Biotechnol.* **2021**, *39*, 1144–1159.
- (16) Giorgi, C.; Marchi, S.; Simoes, I. C. M.; Ren, Z.; Morciano, G.; Perrone, M.; Patalas-Krawczyk, P.; Borchard, S.; Jędrak, P.; Pierzynowska, K.; Szymański, J.; Wang, D. Q.; Portincasa, P.; Węgrzyn, G.; Zischka, H.; Dobrzyn, P.; Bonora, M.; Duszynski, J.; Rimessi, A.; Karkucinska-Wieckowska, A.; et al. Mitochondria and Reactive Oxygen Species in Aging and Age-Related Diseases. *Int. Rev. Cell Mol. Biol.* **2018**, *340*, 209–344.
- (17) Sies, H.; Belousov, V.; Chandel, N. S.; Davies, M. J.; Jones, D. P.; Mann, G. E.; Murphy, M. P.; Yamamoto, M.; Winterbourn, C. Defining Roles of Specific Reactive Oxygen Species (ROS) in Cell Biology and Physiology. *Nat. Rev. Mol. Cell Biol.* **2022**, *23*, 499–515.
- (18) Foret, M. K.; Lincoln, R.; do Carmo, S.; Cuello, A. C.; Cosa, G. Connecting the “Dots”: From Free Radical Lipid Autoxidation to Cell Pathology and Disease. *Chem. Rev.* **2020**, *120*, 12757–12787.
- (19) Panov, A. Peroxyl Radical (HO₂•) as Inducer of the Isoprostane Lipid Peroxidation in Mitochondria. *Mol. Biol.* **2018**, *52*, 295–305.
- (20) Soloviev, M.; Moskalenko, I.; Pliss, E. Quantum Chemical Evaluation of the Role of HO₂• Radicals in the Kinetics of the Methyl Linoleate Oxidation in Micelles. *React. Kinet., Mech. Catal.* **2019**, *127*, 561–581.
- (21) Harrison, K. A.; Haidasz, E. A.; Griesser, M.; Pratt, D. A. Inhibition of Hydrocarbon Autoxidation by Nitroxide-Catalyzed Cross-Dismutation of Hydroperoxyl and Alkylperoxyl Radicals. *Chem. Sci.* **2018**, *9*, 6068–6079.
- (22) Guo, Y.; Baschieri, A.; Mollica, F.; Valgimigli, L.; Cedrowski, J.; Litwinienko, G.; Amorati, R. Hydrogen Atom Transfer from HOO• to Ortho-Quinones Explains the Antioxidant Activity of Polydopamine. *Angew. Chem., Int. Ed.* **2021**, *60*, 15220–15224.
- (23) Baschieri, A.; Valgimigli, L.; Gabbanini, S.; Dilabio, G. A.; Romero-Montalvo, E.; Amorati, R. Extremely Fast Hydrogen Atom Transfer between Nitroxides and HOO• Radicals and Implication for Catalytic Coantioxidant Systems. *J. Am. Chem. Soc.* **2018**, *140*, 10354–10362.
- (24) Astete, C. E.; Dolliver, D.; Whaley, M.; Khachatryan, L.; Sabliov, C. M. Antioxidant Poly(Lactic-Co-Glycolic) Acid Nanoparticles Made with α -Tocopherol-Ascorbic Acid Surfactant. *ACS Nano* **2011**, *5*, 9313–9325.
- (25) Jalilov, A. S.; Nilewski, L. G.; Berka, V.; Zhang, C.; Yakovenko, A. A.; Wu, G.; Kent, T. A.; Tsai, A. L.; Tour, J. M. Perylene Diimide as a Precise Graphene-like Superoxide Dismutase Mimetic. *ACS Nano* **2017**, *11*, 2024–2032.
- (26) Huang, B.; Mao, L.; Shi, X.; Yang, H. B. Recent Advances and Perspectives on Supramolecular Radical Cages. *Chem. Sci.* **2021**, *12*, 13648–13663.
- (27) Tang, B.; Zhao, J.; Xu, J. F.; Zhang, X. Tuning the Stability of Organic Radicals: From Covalent Approaches to Non-Covalent Approaches. *Chem. Sci.* **2020**, *11*, 1192–1204.
- (28) Shilovskikh, V. V.; Timralieva, A. A.; Belogub, E. V.; Konstantinova, E. A.; Kokorin, A. I.; Skorb, E. V. Radical Activity of Binary Melamine-Based Hydrogen-Bonded Self-Assemblies. *Appl. Magn. Reson.* **2020**, *51*, 939–949.
- (29) Shilovskikh, V. V.; Timralieva, A. A.; Nesterov, P. V.; Novikov, A. S.; Sitnikov, P. A.; Konstantinova, E. A.; Kokorin, A. I.; Skorb, E. V. Melamine–Barbiturate Supramolecular Assembly as a pH-Dependent Organic Radical Trap Material. *Chem. – Eur. J.* **2020**, *26*, 16603–16610.
- (30) Ivatt, P. D.; Evans, M. J.; Lewis, A. C. Suppression of Surface Ozone by an Aerosol-Inhibited Photochemical Ozone Regime. *Nat. Geosci.* **2022**, *15*, 536–540.
- (31) Sena, L. A.; Chandel, N. S. Physiological Roles of Mitochondrial Reactive Oxygen Species. *Mol. Cell* **2012**, *48*, 158–167.
- (32) Dröge, W. Free Radicals in the Physiological Control of Cell Function. *Physiol. Rev.* **2002**, *82*, 47–95.
- (33) Cedrowski, J.; Litwinienko, G.; Baschieri, A.; Amorati, R. Hydroperoxyl Radicals (HOO•): Vitamin E Regeneration and H-Bond Effects on the Hydrogen Atom Transfer. *Chem. – Eur. J.* **2016**, *22*, 16441–16445.
- (34) Chong, Y.; Ge, C.; Fang, G.; Tian, X.; Ma, X.; Wen, T.; Wamer, W. G.; Chen, C.; Chai, Z.; Yin, J. J. Crossover between Anti- and Pro-Oxidant Activities of Graphene Quantum Dots in the Absence or Presence of Light. *ACS Nano* **2016**, *10*, 8690–8699.
- (35) Li, Y.; Zhang, W.; Niu, J.; Chen, Y. Mechanism of Photo-generated Reactive Oxygen Species and Correlation with the Antibacterial Properties of Engineered Metal-Oxide Nanoparticles. *ACS Nano* **2012**, *6*, 5164–5173.
- (36) Cilento, G.; Adam, W. From free radicals to electronically excited species. *Free Radical Biol. Med.* **1995**, *19*, 103–114.
- (37) Miyamoto, S.; Martinez, G. R.; Medeiros, M. H. G.; di Mascio, P. Singlet Molecular Oxygen Generated by Biological Hydroperoxides. *J. Photochem. Photobiol. B* **2014**, *139*, 24–33.
- (38) Delchev, V. B.; Ivanova, I. P. Theoretical Study of the Excited-State Reaction Paths of the OH and NH Dissociation Processes in Barbituric Acid. *Monatsh. Chem.* **2012**, *143*, 1141–1150.
- (39) Nesterov, P. V.; Shilovskikh, V. V.; Sokolov, A. D.; Gurzhiy, V. V.; Novikov, A. S.; Timralieva, A. A.; Belogub, E.; Kondratyuk, N. D.; Orekhov, N. D.; Skorb, E. V. Encapsulation of Rhodamine 6G Dye Molecules for Affecting Symmetry of Supramolecular Crystals of Melamine-Barbiturate. *Symmetry* **2021**, *13*, 1119.
- (40) Orekhov, N.; Kondratyuk, N.; Logunov, M.; Timralieva, A.; Shilovskikh, V.; Skorb, E. V. Insights into the Early Stages of Melamine Cyanurate Nucleation from Aqueous Solution. *Cryst. Growth Des.* **2021**, *21*, 1984–1992.
- (41) Abdurahman, A.; Hele, T. J. H.; Gu, Q.; Zhang, J.; Peng, Q.; Zhang, M.; Friend, R. H.; Li, F.; Evans, E. W. Understanding the Luminescent Nature of Organic Radicals for Efficient Doublet Emitters and Pure-Red Light-Emitting Diodes. *Nat. Mater.* **2020**, *19*, 1224–1229.
- (42) Bedard, L.; Young, M. J.; Hall, D.; Paul, T.; Ingold, K. U. Quantitative Studies on the Peroxidation of Human Low-Density Lipoprotein Initiated by Superoxide and by Charged and Neutral Alkylperoxyl Radicals. *J. Am. Chem. Soc.* **2001**, *123*, 12439–12448.
- (43) Neese, F.; Wiley, J. The ORCA Program System. *Wiley Interdiscip. Rev. Comput. Mol. Sci.* **2012**, *2*, 73–78.
- (44) Neese, F.; Wennmohs, F.; Hansen, A.; Becker, U.; Neese, F.; Wennmohs, F.; Hansen, A.; Becker, U. Efficient, Approximate and Parallel Hartree-Fock and Hybrid DFT Calculations. A ‘Chain-of-Spheres’ Algorithm for the Hartree-Fock Exchange. *Chem. Phys.* **2009**, *356*, 98–109.
- (45) Neese, F. An Improvement of the Resolution of the Identity Approximation for the Formation of the Coulomb Matrix. *J. Comput. Chem.* **2003**, *24*, 1740–1747.
- (46) Berendsen, H. J. C.; van der Spoel, D.; van Drunen, R. GROMACS: A message-passing parallel molecular dynamics implementation. *Comput. Phys. Commun.* **1995**, *91*, 43–56.
- (47) Eastman, P.; Swails, J.; Chodera, J. D.; McGibbon, R. T.; Zhao, Y.; Beauchamp, K. A.; Wang, L. P.; Simmonett, A. C.; Harrigan, M. P.; Stern, C. D.; Wiewiora, R. P.; Brooks, B. R.; Pande, V. S. OpenMM 7: Rapid Development of High Performance Algorithms for Molecular Dynamics. *PLoS Comput. Biol.* **2017**, *13*, No. e1005659.

(48) Jorgensen, W. L.; Maxwell, D. S.; Tirado-Rives, J. Development and testing of the OPLS all-atom force field on conformational energetics and properties of organic liquids. *J. Am. Chem. Soc.* **1996**, *118*, 11225–11236.

(49) Jorgensen, W. L.; Tirado-Rives, J. Potential energy functions for atomic-level simulations of water and organic and biomolecular systems. *Proc. Natl. Acad. Sci. U.S.A.* **2005**, *102*, 6665–6670.

(50) Dodda, L. S.; Vilseck, J. Z.; Tirado-Rives, J.; Jorgensen, W. L. 1.14*CM1A-LBCC: Localized bond-charge corrected CM1A charges for condensed-phase simulations. *J. Phys. Chem. B* **2017**, *121*, 3864–3870.

(51) Dodda, L. S.; De Vaca, I. C.; Tirado-Rives, J.; Jorgensen, W. L. LigParGen web server: An automatic OPLS-AA parameter generator for organic ligands. *Nucleic Acids Res.* **2017**, *45*, W331–W336.

(52) Jorgensen, W. L.; Chandrasekhar, J.; Madura, J. D.; Impey, R. W.; Klein, M. L. Comparison of simple potential functions for simulating liquid water. *J. Chem. Phys.* **1983**, *79*, 926–935.

(53) Essmann, U.; Perera, L.; Berkowitz, M. L.; Darden, T.; Lee, H.; Pedersen, L. G. A smooth particle mesh Ewald method. *J. Chem. Phys.* **1995**, *103*, 8577–8593.

(54) Brehm, M.; Kirchner, B. TRAVIS-A free analyzer and visualizer for monte carlo and molecular dynamics trajectories. *J. Chem. Inf. Model.* **2011**, *51*, 2007–2023.